

Linear algebraic calculation of the Green's function for large-scale electronic structure theory

R. Takayama,^{1,2,*} T. Hoshi,^{2,3} T. Sogabe,^{2,†} S.-L. Zhang,^{2,†} and T. Fujiwara^{2,3}

¹Research and Development for Applying Advanced Computational Science and Technology (ACT-JST), Japan Science and Technology Agency, 4-1-8 Honcho, Kawaguchi-shi, Saitama 332-0012, Japan

²Department of Applied Physics, University of Tokyo, 7-3-1 Hongo, Bunkyo-ku, Tokyo 113-8656, Japan

³Core Research for Evolutional Science and Technology (CREST-JST),

Japan Science and Technology Agency, 4-1-8 Honcho, Kawaguchi-shi, Saitama 332-0012, Japan

(Received 23 March 2005; revised manuscript received 14 December 2005; published 7 April 2006)

A linear algebraic method named the shifted conjugate-orthogonal conjugate-gradient method is introduced for large-scale electronic structure calculation. The method gives an iterative solver algorithm of the Green's function and the density matrix without calculating eigenstates. The problem is reduced to independent linear equations at many energy points and the calculation is actually carried out only for a single energy point. The method is robust against the round-off error and the calculation can reach the machine accuracy. With the observation of residual vectors, the accuracy can be controlled, microscopically, independently for each element of the Green's function, and dynamically, at each step in dynamical simulations. The method is applied to both a semiconductor and a metal.

DOI: [10.1103/PhysRevB.73.165108](https://doi.org/10.1103/PhysRevB.73.165108)

PACS number(s): 71.15.-m, 71.15.Nc, 71.15.Pd

I. INTRODUCTION

Large-scale atomistic simulation with quantum mechanical freedom of electrons requires manipulation of a large Hamiltonian matrix. In order to calculate the physical quantities of a system, we should obtain either eigenstates or the density matrix of the system. The calculation of eigenstates is usually reduced to a matrix diagonalization procedure and this procedure results in severe computational cost for a large-scale system.

Any physical quantity X can be evaluated by means of the density matrix ρ as

$$\langle X \rangle = \int \int d\mathbf{r} d\mathbf{r}' \rho(\mathbf{r}, \mathbf{r}') X(\mathbf{r}', \mathbf{r}). \quad (1)$$

Even though the density matrix is of long range, only the short-range behavior of the density matrix is necessary, if X is a short-range operator. The energy and forces acting on an individual atom are really this case, and the locality of the Hamiltonian realizes this feature in large-scale calculation. Moreover, the density matrix ρ can be obtained from the Green's function. Therefore, the essential methodology for large-scale electronic structure calculation and molecular dynamics (MD) simulation is how to obtain the density matrix ρ or Green's function without calculating eigenstates.¹⁻¹⁵

We have developed a set of methods for large-scale atomistic simulation without calculating eigenstates in a fully quantum mechanical description of electron systems.⁶⁻¹² Among them, the subspace diagonalization method based on the Krylov subspace (SDKS method) was introduced, where the original Hamiltonian matrix H is reduced to a small-size easily tractable one and its diagonalization leads to approximation of the density matrix of the original system.¹¹ The first important feature of the SDKS method is that we can monitor numerical accuracy during the simulation using a residual error of the Green's function, as shown in the present paper. The second important feature is that the SDKS

method can be used both for metallic and insulating systems. We found, however, that the SDKS method has a numerical instability, when the energy spectrum is calculated with a *very fine* energy resolution, as discussed in the Appendix.

Then our strategy to obtain the Green's function and the density matrix is to solve linear equations with a given basis $|j\rangle$:

$$(z - H)|x_j\rangle = |j\rangle. \quad (2)$$

In the present case, the Hamiltonian H is real symmetric and $(z - H)$ is not Hermitian but complex symmetric with a complex energy ($z \equiv E + i\gamma$). Once the linear equation is solved, one can obtain any element of the Green's function as

$$G_{ij}(z) = \langle i|(z - H)^{-1}|j\rangle = \langle i|x_j\rangle. \quad (3)$$

Numerical energy integration is required to obtain the one-body density matrix;

$$\rho_{ij} = -\frac{1}{\pi} \int_{-\infty}^{\infty} \text{Im} G_{ij}(E + i\gamma) f\left(\frac{E - \mu}{k_B \tau}\right) dE, \quad (4)$$

with the Fermi distribution function $f(x)$ and a small imaginary part of the energy ($\gamma \rightarrow 0+$). The chemical potential μ is determined so that the sum of the diagonal elements of the density matrix equals the total number of electrons.

The aim of the present paper is to introduce the shifted conjugate-orthogonal conjugate-gradient (COCG) method, an iterative solver algorithm of Eq. (2). The Green's function and the density matrix are obtained using Eqs. (3) and (4). The shifted COCG method shares the before-mentioned two features with the SDKS method. Moreover, the third important feature of the shifted COCG method, different from the SDKS method, is the robustness against round-off error; the calculation can reach machine accuracy.

The present paper is organized as follows. In Sec. II, the Krylov subspace will be explained and the shifted COCG method will be introduced. In Sec. III, the residual norm

(RN) will be introduced to monitor the convergence behavior of the method. The number of operations in actual calculation is also discussed. Section IV is devoted to application of the present method to an atomic-scale reconstruction of a semiconductor surface (silicon) and the bulk electronic structure of a metal (copper). The conclusion will be given in Sec. V. In the Appendix, several numerical aspects will be discussed for the shifted COCG and SDKS methods and the difference between the two methods will be clarified.

II. SHIFTED CONJUGATE-ORTHOGONAL CONJUGATE-GRADIENT METHOD

A. Shifted systems and Krylov subspace

Now we should concentrate the method to solve Eq. (2) with a large matrix H and a fixed basis $|j\rangle$. The method should be iterative and not require the matrix inversion procedure of $(z-H)$. The problem is reduced to the linear equations Eq. (2) for a given set of energy points $z=z_1, z_2, z_3, \dots$. These linear equations are called “shifted” linear equations or “shifted” linear systems in mathematical textbooks, because shifted matrices $(z_1-H), (z_2-H), (z_3-H), \dots$ appear. If the equations are solved independently among different energy points, the total computational cost is proportional to the number of energy points N_{ene} . The essence of the present method is that we should solve the equation only at one energy point and the solutions at other energy points are given with a moderate computational cost.

The present method is realized using the Krylov subspace.^{16,17} The Krylov subspace is defined for an arbitrary matrix A and vector $|j\rangle$ as the linear space spanned by a set of states (vectors) $\{A^n|j\rangle\}$:

$$K_n(A, |j\rangle) \equiv \text{span}\{|j\rangle, A|j\rangle, A^2|j\rangle, \dots, A^{n-1}|j\rangle\}, \quad (5)$$

where n is the dimension of the KS. Iterative methods based on the KS, such as the standard conjugate-gradient algorithm, are generally called Krylov subspace methods. In the present method, the solution vector $|x_j\rangle$ of Eq. (2) is constructed within the KS of $K_n(z-H, |j\rangle)$ at the n th iteration.

The present method, the shifted COCG method, is a combined method of two KS algorithms: (a) the conjugate-orthogonal conjugate-gradient method¹⁸ and (b) the theorem of collinear residuals for shifted linear systems.¹⁹ The essential point is that the KS among shifted systems gives the same linear space

$$K_n(z_1-H, |j\rangle) = K_n(z_2-H, |j\rangle). \quad (6)$$

The actual procedures are given in the next section.

B. Shifted COCG method

Here we present the formulation of the shifted COCG algorithm, following Ref. 19. We pick out arbitrarily one energy point as the “reference” energy point $z_{\text{ref}} \equiv E_{\text{ref}} + i\gamma$. Equation (2) at the reference energy ($z=z_{\text{ref}}$) is reformulated as

$$Ax = b, \quad (7)$$

where the matrix A is defined as $A \equiv z_{\text{ref}} - H$ and the suffix j is dropped ($|j\rangle \Rightarrow \mathbf{b}, |x_j\rangle \Rightarrow \mathbf{x}$). Since the matrix A is not Her-

mitian, the matrix-vector notation is used in this section, rather than the bracket notation. Hereafter the equation at $z=z_{\text{ref}}$ is called the reference system.

For Eq. (7), we use the COCG algorithm,¹⁸ a standard iterative algorithm for a linear equation with a complex symmetric matrix A .²⁰ At the n th iteration, the solution vector \mathbf{x}_n , the residual vector \mathbf{r}_n , and the search direction vector \mathbf{p}_n are represented as

$$\mathbf{x}_n = \mathbf{x}_{n-1} + \alpha_{n-1}\mathbf{p}_{n-1}, \quad (8)$$

$$\mathbf{r}_n = \mathbf{r}_{n-1} - \alpha_{n-1}A\mathbf{p}_{n-1}, \quad (9)$$

$$\mathbf{p}_n = \mathbf{r}_n + \beta_{n-1}\mathbf{p}_{n-1}, \quad (10)$$

respectively. Here, the coefficients α_n and β_n are given as

$$\alpha_n = \frac{\mathbf{r}_n^T \mathbf{r}_n}{\mathbf{p}_n^T A \mathbf{p}_n}, \quad (11)$$

$$\beta_n = \frac{\mathbf{r}_{n+1}^T \mathbf{r}_{n+1}}{\mathbf{r}_n^T \mathbf{r}_n}. \quad (12)$$

The initial conditions for iteration are $\mathbf{x}_0 = \mathbf{p}_{-1} = 0$, $\mathbf{r}_0 = \mathbf{b}$, $\beta_{-1} = 0$, $\alpha_{-1} = 1$. Note here that the inner products are given as $\mathbf{a}^T \mathbf{b}$ ($\neq \mathbf{a}^H \mathbf{b}$). When the iteration number n reaches the matrix dimension of A , denoted M , the residual vector should be zero and the solution vector should be exact ($\mathbf{r}_M = 0, \mathbf{x}_M = A^{-1}\mathbf{b}$).

Eliminating \mathbf{p}_{n-1} from Eq. (9) with Eq. (10), we obtain a three-term recurrence relation for the residual vector,

$$\mathbf{r}_{n+1} = -\alpha_n A \mathbf{r}_n + \left(1 + \frac{\beta_{n-1} \alpha_n}{\alpha_{n-1}}\right) \mathbf{r}_n - \frac{\beta_{n-1} \alpha_n}{\alpha_{n-1}} \mathbf{r}_{n-1}. \quad (13)$$

The most time-consuming part of the COCG algorithm is calculating the matrix-vector product ($A\mathbf{p}_n$) in Eq. (11). This matrix-vector product corresponds to the procedure for updating the KS: $K_n(A, \mathbf{b}) \Rightarrow K_{n+1}(A, \mathbf{b})$.

Similarly, we reformulate Eq. (2) with a shifted energy point $z = z_{\text{ref}} + \sigma$ as

$$(A + \sigma I)\mathbf{x} = \mathbf{b}. \quad (14)$$

For the shifted system, the n th solution vector \mathbf{x}_n^σ and the search direction vector \mathbf{p}_n^σ are given as

$$\mathbf{x}_n^\sigma = \mathbf{x}_{n-1}^\sigma + \alpha_{n-1}^\sigma \mathbf{p}_{n-1}^\sigma, \quad (15)$$

$$\mathbf{p}_n^\sigma = \mathbf{r}_n^\sigma + \beta_{n-1}^\sigma \mathbf{p}_{n-1}^\sigma. \quad (16)$$

The initial values of the vectors or coefficients are chosen to be the same as in the reference system. The equation corresponding to Eq. (13) of the shifted system is

$$\mathbf{r}_{n+1}^\sigma = -\alpha_n^\sigma (A + \sigma I) \mathbf{r}_n^\sigma + \left(1 + \frac{\beta_{n-1}^\sigma \alpha_n^\sigma}{\alpha_{n-1}^\sigma}\right) \mathbf{r}_n^\sigma - \frac{\beta_{n-1}^\sigma \alpha_n^\sigma}{\alpha_{n-1}^\sigma} \mathbf{r}_{n-1}^\sigma. \quad (17)$$

Since the KSs of the reference and shifted systems are equivalent [$K_n(A, \mathbf{b}) = K_n(A + \sigma I, \mathbf{b})$], as stated in Eq. (6), one can prove that their residual vectors \mathbf{r}_n^σ and \mathbf{r}_n are collinear:

$$\mathbf{r}_n^\sigma = \frac{1}{\pi_n^\sigma} \mathbf{r}_n. \quad (18)$$

which is the theorem of the collinear residual for shifted linear systems.¹⁹ With Eq. (18), Eq. (13) can be modified as

$$\begin{aligned} \mathbf{r}_{n+1}^\sigma = & -\frac{\pi_n^\sigma}{\pi_{n+1}^\sigma} \alpha_n (A + \sigma I) \mathbf{r}_n^\sigma + \frac{\pi_n^\sigma}{\pi_{n+1}^\sigma} \left(1 + \alpha_n \sigma + \frac{\beta_{n-1} \alpha_n}{\alpha_{n-1}} \right) \mathbf{r}_n^\sigma \\ & - \frac{\pi_{n-1}^\sigma}{\pi_{n+1}^\sigma} \frac{\beta_{n-1} \alpha_n}{\alpha_{n-1}} \mathbf{r}_{n-1}^\sigma. \end{aligned} \quad (19)$$

Comparing the coefficients in Eqs. (19) and (17), we obtain

$$\alpha_n^\sigma = \frac{\pi_n^\sigma}{\pi_{n+1}^\sigma} \alpha_n, \quad (20)$$

$$\beta_n^\sigma = \left(\frac{\pi_n^\sigma}{\pi_{n+1}^\sigma} \right)^2 \beta_n, \quad (21)$$

$$\pi_{n+1}^\sigma = \left(1 + \alpha_n \sigma + \frac{\beta_{n-1} \alpha_n}{\alpha_{n-1}} \right) \pi_n^\sigma - \frac{\beta_{n-1} \alpha_n}{\alpha_{n-1}} \pi_{n-1}^\sigma \quad (22)$$

with the initial values of $\pi_0^\sigma = \pi_{-1}^\sigma = 1$. We can update the vector \mathbf{r}_n^σ and the coefficients α_n^σ and β_n^σ using Eqs. (18) and (20)–(22) which *do not* include any matrix-vector product. Consequently, the time-consuming procedure of the matrix-vector product is needed only for the reference system, which reduces the computational cost drastically. The detail of the computational cost will be estimated in Sec. III B.

We note here that the shift parameter σ ($\equiv z - z_{\text{ref}}$) is an arbitrary complex variable in principle but we choose the value to be real ($\sigma = E - E_{\text{ref}}$) in all the practical calculations of the present paper. We also note that a practical electronic-structure calculation can be parallelized with the present method, because the original problem of Eq. (2) is independent with respect to the basis suffix j .

III. CONVERGENCE BEHAVIOR AND COMPUTATIONAL COST

A. Convergence behavior with residual norm

Since the shifted COCG method is an iterative solver algorithm for Eq. (2), we should establish a systematic procedure to find an optimal iteration number in the context of electronic structure calculation. In this section, such a systematic procedure is introduced by monitoring the norm of residual vector.

At the n th iteration, we denote the solution vectors for the reference and shifted systems as $|x_n^{(j)}\rangle$ and $|x_n^{\sigma(j)}\rangle$, respectively. The corresponding residual vectors are written by

$$|r_n^{(j)}\rangle \equiv |j\rangle - (z_{\text{ref}} - H) |x_n^{(j)}\rangle, \quad (23)$$

$$|r_n^{\sigma(j)}\rangle \equiv |j\rangle - (z_{\text{ref}} + \sigma - H) |x_n^{\sigma(j)}\rangle = \frac{1}{\pi_n^\sigma} |r_n^{(j)}\rangle, \quad (24)$$

respectively. The last equality is given by Eq. (18).

Since we need only the elements of the density matrix among near-sited orbital pairs or of the short-distance com-

ponents in Eq. (1), the convergence is necessary only for these components, but not for far-distance components. Therefore, we define a residual norm from the components only among these near-sited orbitals ($|i\rangle$) that are determined by the interaction range of Hamiltonian:

$$\|r_n^{(j)}\|^2 \equiv \sum_i^{M_{\text{int}}} |\langle i | r_n^{(j)} \rangle|^2, \quad (25)$$

$$\|r_n^{\sigma(j)}\|^2 \equiv \sum_i^{M_{\text{int}}} |\langle i | r_n^{\sigma(j)} \rangle|^2 = \left| \frac{1}{\pi_n^\sigma} \right|^2 \|r_n^{(j)}\|^2, \quad (26)$$

where M_{int} is the number of interacting orbitals $|i\rangle$ for a basis $|j\rangle$, typically 10–10². Note that the RN is an energy-dependent quantity.

Since the Green's function should be integrated over the given set of energy points to obtain the density matrix, we need to know the convergence behavior of the RN over the entire energy range. Then we average the RN over the energy range ($E_{\text{min}} < E < E_{\text{max}}$ or $E_{\text{min}} - E_{\text{ref}} < \sigma < E_{\text{max}} - E_{\text{ref}}$). We call the resultant quantity the energy-averaged residual norm (ARN),

$$R_n^{(j)} \equiv \frac{1}{E_{\text{max}} - E_{\text{min}}} \int_{E_{\text{min}}}^{E_{\text{max}}} dE \|r_n^{\sigma(j)}\|^2 = \xi_n^{(j)} \|r_n^{(j)}\|^2, \quad (27)$$

where

$$\xi_n^{(j)} = \frac{1}{E_{\text{max}} - E_{\text{min}}} \int_{E_{\text{min}}}^{E_{\text{max}}} \left| \frac{1}{\pi_n^\sigma} \right|^2 dE. \quad (28)$$

Since the ARN $R_n^{(j)}$ can be monitored at every iteration (n), the optimal number of iterations can be determined by the value of $R_n^{(j)}$. The above determination is carried out for the *microscopic* freedoms or individually among the basis suffixes j .

As an example, we calculated the electronic structure in a bulk Si system of 512 atoms with a cubic simulation cell. We use a transferable Hamiltonian of silicon in the Slater-Koster form of s and p orbitals.²¹ The matrix dimension of the Hamiltonian H is $M = 4 \times 512 = 2048$ and the number of energy points is $N_{\text{ene}} = 1000$. The imaginary part of the energy ($z = E + i\gamma$) is set to $\gamma = 0.002$ a.u. ($= 0.0544$ eV). Figure 1 shows the decay behavior of the ARN. Here and hereafter, the starting basis $|j\rangle$ for silicon systems is set to an sp^3 -hybridized basis on an atom. We plot four cases with different reference energy points. In the result, all the cases follow a universal curve up to the machine accuracy, and the choice of the reference energy point does not affect the calculated ARN. The behavior within a small iteration ($n \leq 70$) is also plotted in Fig. 2. We should note that the observed decay at the early stage ($n \leq 30$) is important from a practical viewpoint, since the iteration number of $n \approx 30$ is enough for the application in Sec. IV A.

The convergence behavior was studied also in bulk fcc Cu of 1568 atoms, a metallic system. The simulation cell is a $7 \times 7 \times 8$ supercell of the cubic unit cell. We constructed the Hamiltonian matrix from the second-order form ($H^{(2)}$) of the tight-binding linear muffin-tin orbital theory.²² In Fig. 2, the

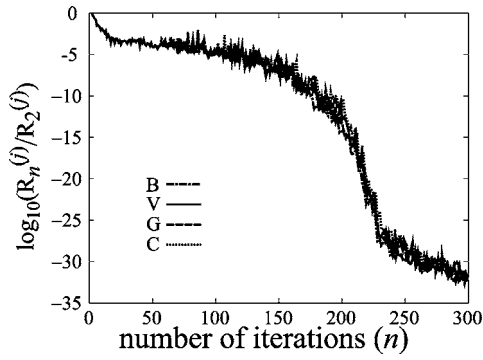


FIG. 1. Decay behavior of the ARN for a Si crystal with 512 atoms. A universal curve appears with four different reference energy points that are placed at the band bottom (B), in the valence band (V), in the gap (G), and in the conduction band (C). See Fig. 6(a) for the actual positions of these energy points.

ARN is plotted with the starting bases of atomic s and t_{2g} orbitals. Since the present method is a general linear algebraic theory with a short-range Hamiltonian (matrix), the convergence behavior shows no generic difference between semiconductor and metal or between different starting orbitals. In fact, the curves in Fig. 2 behave similarly in magnitude with a large iteration number, for example $n \geq 60$, though differently with a smaller iteration number.

B. Computational cost within one iteration

Numbers of operations within one iteration are estimated in Table I. Two points are found for the drastic reduction of computational cost, when the present method is compared to the conventional COCG method. For comparison, the case of the conventional COCG method is shown in the row labeled COCG, in which the conventional COCG method is applied, independently, to all the systems (N_{ene} systems) and the matrix-vector product governs the computational cost. In the shifted COCG method, on the other hand, the computational cost of the matrix-vector product is reduced by $1/N_{\text{ene}}$ ($MM_{\text{int}}N_{\text{ene}} \Rightarrow MM_{\text{int}}$), since the actual matrix-vector product is carried out only for the reference system, as discussed in

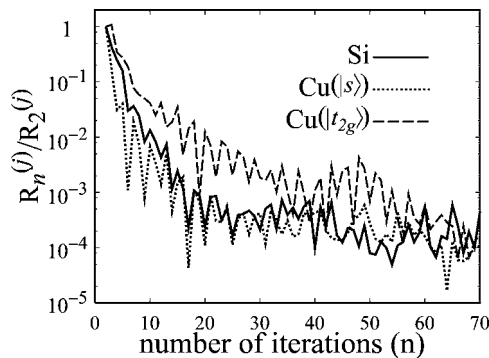


FIG. 2. Early stage in the decay behavior of the ARN for a Si crystal with 512 atoms and fcc Cu with 1568 atoms. In the Cu system, the two cases are plotted with the starting vectors $|j\rangle$ of s and t_{2g} bases on an atom.

TABLE I. Numbers of operations within one iteration: (i) Inner product in Eqs. (11) and (12), (ii) scalar-vector product in Eqs. (8)–(10) and Eqs. (15), (16), and (18), and (iii) matrix-vector product in Ap_n of Eq. (11). The parameters in the table are as follows: M , the dimension of the original Hamiltonian matrix; M_{int} , the number of orbitals within interaction range for one orbital; N_{ene} , the number of energy points. Here, the cases of the three methods are plotted; (1) the conventional COCG method, labeled COCG, (2) the shifted COCG method with the calculation of *all* the elements of the Green's function and the RN, labeled SCOCG (total), and (3) the actual procedure in the present calculation, labeled SCOCG (present). See the text for details.

Method	Inner product	Scalar-vector product	Matrix-vector product
COCG	$3MN_{\text{ene}}$	$3MN_{\text{ene}}$	$MM_{\text{int}}N_{\text{ene}}$
SCOCG (total)	$3M$	$3MN_{\text{ene}}$	MM_{int}
SCOCG (present)	$3M$	$3M_{\text{int}}(N_{\text{ene}}-1)+3M$	MM_{int}

Sec. II B. Then the scalar-vector products may give a significant contribution to the computation, if all the elements (M elements) of the vectors x_n^σ , p_n^σ , and r_n^σ are calculated for all the systems, which is shown in the row labeled SCOCG (total). In the present calculation, however, we need the elements of these vectors only within the interaction range (M_{int} elements), as discussed in Sec. III A. Since the vectors x_n^σ , p_n^σ , and r_n^σ in the shifted systems ($N_{\text{ene}}-1$ systems) are updated using Eqs. (15), (16), and (18), the update procedure can be carried out only for the necessary elements (M_{int} elements). The calculation only for these elements gives another drastic reduction of the computation cost [$3M(N_{\text{ene}}-1) \Rightarrow 3M_{\text{int}}(N_{\text{ene}}-1)$], which is shown in the row labeled SCOCG (present).

IV. APPLICATIONS TO ELECTRONIC STRUCTURE CALCULATION

A. Reconstruction on Si(001) surface

The MD simulation with the shifted COCG method was tested in a Si(001) surface reconstruction. The calculated system is a slab of 1024 atoms constituted of 16 layers with 64 atoms on each layer. The temperature parameter of the Fermi distribution function in Eq. (4) is set to $\tau=0.005$ a.u. ($=0.136$ eV). We use the Hamiltonian and energy function in Ref. 21. Other methodological details are the same as in Sec. III A. The atomic structure is relaxed, with the Hellmann-Feynman force on atoms, from an appropriate surface atomic configuration into the ground-state structure. Since the force on atoms is given after the calculation of the density matrix, the simulation is carried out by a double-loop iterative procedure. The inner loop is the iterative procedure of the shifted COCG method for calculating the density matrix with a given atomic configuration or a given Hamiltonian. The outer loop is the update of the atomic configuration, with the force on atoms, so as to minimize the energy. When the KS dimension, or the iteration number of the inner loop, is n

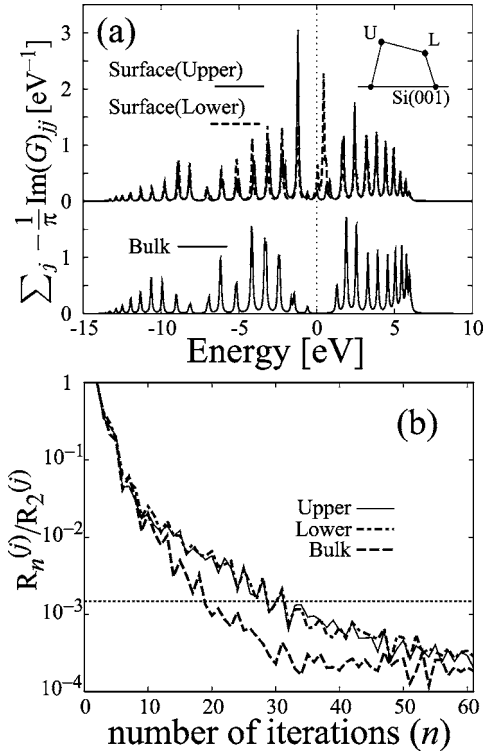


FIG. 3. Result of a slab for the Si(001) surface with asymmetric surface dimers. (a) Local density of states $[\sum_j - (1/\pi) \text{Im} G_{jj}]$ for surface and bulk atoms, calculated with the KS dimension of $n = 30$. The surface atoms are classified into the upper and lower atoms of the asymmetric dimer, illustrated in the inset. The “bulk” atom is an atom on deeper layers of the present slab system. (b) Decay behavior of ARN for the atoms that appear in (a). The horizontal dotted line is a guide for the eye for a typical convergence criterion.

$= 30$ or larger, the resultant surface atoms form asymmetric dimers illustrated in the inset of Fig. 3(a), as they should do.^{23,24} The resultant tilt angle of the asymmetric dimers is $\theta = 13.4^\circ$, which agrees with experimental values of θ , between 5° and 19° .²⁵

Figure 3(a) shows the imaginary part of the Green’s function $\sum_j - (1/\pi) \text{Im} G_{jj}$ summed up over the orbitals within a specific atom, which corresponds to the local density of states (LDOS). As a general property of the KS method, the number of peaks in $-(1/\pi) \text{Im} G_{jj}$ equals the iteration number or the KS dimension. When the LDOSs of the surface and bulk atoms are compared, the LDOSs of the surface atoms have characteristic peaks within $-1 \leq E \leq +0.5$ eV, because the upper surface atom has an *occupied* surface state and the lower one has an *unoccupied* surface state. The reproduction of these surface states is the reason why the correct surface reconstruction is reproduced, even with a small number of the KS dimension ($n = 30$).

Figure 3(b) shows the ARN for these atoms as the function of the iteration number or the KS dimension. Here the ARN for an atom is defined as the average of the ARN, Eq. (27), among the orbitals within the atom. The result shows that the ARN for the surface atoms decays similarly, while that for the bulk atom decays faster. Considering the fact that

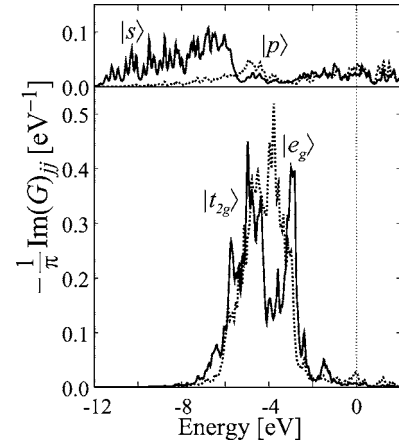


FIG. 4. Result for fcc Cu with 1568 atoms: Partial density of states $-(1/\pi) \text{Im} G_{jj}$ for each orbital.

the required number of iterations is $n = 30$ to obtain appropriate surface reconstruction, a practical convergence criterion is estimated as the horizontal dotted line in Fig. 3(b) on the order of $R_n^{(j)}/R_2^{(j)} \sim 10^{-3}$. If this convergence criterion is used, the optimal number of iterations is approximately 18 for the bulk atom, and less than that for the surface atoms ($n = 30$). In other words, the optimal iteration number is determined for microscopic degrees of freedom or independently among atoms or bases ($|j\rangle$). Moreover, the microscopic control can be carried out dynamically, or at every step in MD simulations. In short, the observation of the ARN gives a definite way of controlling the accuracy microscopically and dynamically, which is important in practical investigations.

B. Metal system: fcc Cu

We calculated also the electronic structure of bulk fcc Cu with 1568 atoms. The technical details are already explained in Sec. III A. The well-converged partial DOS is shown in Fig. 4 for s , p , e_g , and t_{2g} orbitals. The result reproduces the essential characteristics, e.g., the resonance behavior of s and p orbitals and the energy separation between e_g and t_{2g} orbitals.

Another important property for analyzing cohesion is the crystal orbital Hamiltonian population (COHP) defined as follows:²⁶

$$C_{IJ;\alpha}(E) = -\frac{1}{\pi} \sum_{\beta} \text{Im} G_{I\alpha;J\beta}(E + i\gamma) H_{J\beta;I\alpha}, \quad (29)$$

$$C_{IJ}(E) = \sum_{\alpha} C_{IJ;\alpha}(E), \quad (30)$$

where I and J denote the atomic positions and α and β the orbitals. The quantity C_{IJ} is the COHP and we call the quantity $C_{IJ;\alpha}$ the partial COHP (PCOHP). The energy integration of the COHP (ICOHP) has the dimension of energy. The off-site term of the ICOHP gives a quantitative measure of the cohesive mechanism, because its negative and positive parts are the energy gain and loss in the electronic structure energy for cohesion, respectively.

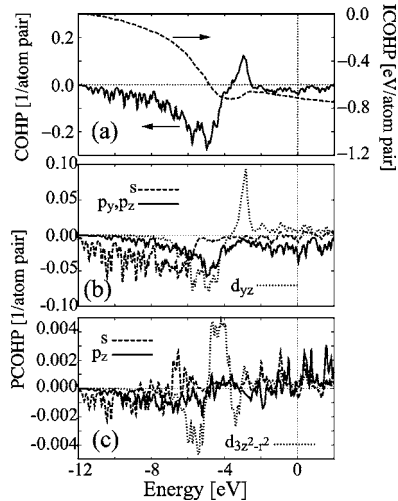


FIG. 5. Result for fcc Cu with 1568 atoms: COHP and ICOHP for a first-nearest-neighbor atom pair (a) and PCOHP for a first- (b) or second- (c) nearest-neighbor atom pair.

Figure 5(a) shows the COHP and ICOHP for a nearest-neighbor atom pair. The PCOHP $C_{IJ;\alpha}(E)$ is also shown in Fig. 5(b) only for the orbitals (α) with major contributions. Since a nearest-neighbor pair lies along the (011) direction in the fcc structure, the significant values in the PCOHP come from $\alpha=s$, $(p_y \pm p_z)/\sqrt{2}$, and d_{yz} orbitals. Figures 5(a) and 5(b) show that the two characteristic peaks of the COHP at $E \approx -5$ and -3 eV are contributed mainly by the PCOHP of the d_{yz} orbital. The negative and positive peaks originate from the bonding and antibonding coupling, respectively, of the t_{2g} orbitals among the nearest-neighbor atom sites. Though the two corresponding peaks can be seen also in the PDOS of the t_{2g} orbital in Fig. 4, the COHP, unlike the PDOS, informs us about the bonding or antibonding character of the corresponding state. From Fig. 5(b), we found that contributions from s and p orbitals are also appreciable. Moreover, the PCOHP for a second-nearest-neighbor pair is plotted in Fig. 5(c). Since a second-nearest-neighbor pair lies along the (001) direction, the significant values in the PCOHP come from s , p_z , and $d_{3z^2-r^2}$ orbitals, though their magnitude is one order smaller than that for the first-neighbor pair.

The present analysis demonstrates that, since the shifted COCG method can give the Green's function with machine accuracy, the resultant spectra reproduce the correct cohesive mechanism, in which the role of each orbital is well described not only for the major contribution from the first-nearest-neighbor coupling but also for a minor contribution from the second-nearest-neighbor coupling.

V. CONCLUDING DISCUSSION

In the present paper, we introduced the shifted COCG method based on the Krylov subspace and used the method as an iterative solver algorithm of the Green's function in large electron systems. We analyzed the convergence behavior by means of the ARN, which establishes a definite way of

controlling accuracy. The theory realizes a practical method not only for MD simulations but also for obtaining the fine-resolution spectra, such as (P)DOS and COHP, without calculating eigenstates. The method was applied to a semiconductor and a metal and the above statements were confirmed numerically.

When the present method is compared with the SDKS method, we conclude that the two KS methods are complementary from a practical viewpoint and we should choose one according to the purpose. If one would like to obtain the Green's function in a very fine energy resolution, the shifted COCG method should be used, because it can reach machine accuracy. On the other hand, as is discussed in Appendix A 2, the SDKS method is suitable for obtaining the density matrix without numerical energy integration of the Green's function, which is a typical situation in MD simulations.

Finally, we point out the generality of the present theory. Since the shifted COCG method is based on a general linear-algebraic theory with large matrices, it is applicable not only to electronic structure calculations with atomic orbital bases but also to calculation with other bases. Moreover, the method may be useful in many theoretical fields other than electronic structure theory, if the theory is reduced to a set of shifted linear equations.

ACKNOWLEDGMENTS

Computation was carried out at the Center for Promotion of Computational Science and Engineering (CCSE) of Japan Atomic Energy Research Institute (JAERI) and also partially carried out at the Supercomputer Center, Institute for Solid State Physics, University of Tokyo. This work is financially supported by a Grant-in-Aid from the Ministry of Education, Culture, Sports, Science and Technology and also by ACT-JST and CREST-JST.

APPENDIX: NUMERICAL ASPECTS OF KRYLOV-SUBSPACE METHODS

This appendix is devoted to several aspects of the two KS methods (i) the shifted COCG method, the main subject of this paper, and (ii) the SDKS method.¹¹ In particular, numerical aspects will be discussed, including robustness against round-off error. Examples are demonstrated with silicon crystals, as in Sec. III.

1. Shifted COCG method

For the shifted COCG method, we discuss (I) the convergence behavior among different energy points and (II) the convergence behavior of the long-distance component of the Green's function. These discussions clarify how and why the present method is so successful.

First, we used the conventional COCG method at all the energy points ($N_{\text{ene}}=1000$ points), so as to investigate the convergence behavior among different energy points. Figure 6(a) shows the imaginary part of the well-converged Green's function, corresponding to the density of states. The spectrum consists of a set of spikes with a finite width, owing to a small imaginary part of the energy ($\gamma=0.002$ a.u.

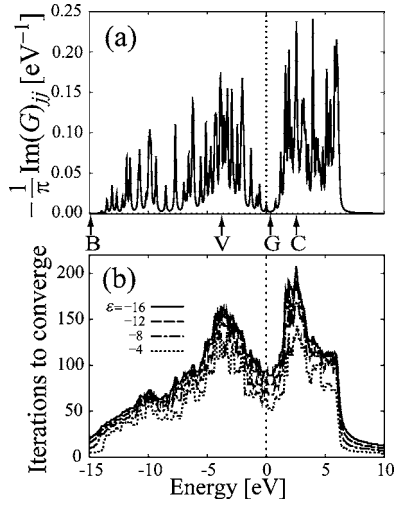


FIG. 6. (a) Well-converged Green's function and (b) convergence behavior at different energy points. The calculation was carried out with 512 Si atoms and the top of the valence band is located at $E=0$ eV (a) imaginary part of the well-converged Green's function $[-(1/\pi)\text{Im} G_{ij}(E+i\gamma)]$ with $\gamma=0.002$ a.u. (b) The iteration numbers to satisfy the converge criterion $\|r_n^{(j)}\|^2 < 10^\varepsilon$ with $\varepsilon=-4$ to -16 . Note that four energy points are picked out, at the band bottom (B), in the valence band (V), in the gap (G), and in the conduction band (C). For discussion, see text.

$=0.0544$ eV). The required iteration numbers with various convergence criteria are seen in Fig. 6(b), in which the convergence criterion is set to be $\|r_n^{(j)}\|^2 < 10^\varepsilon$ with $\varepsilon=-4$ to -16 . The resultant DOS profiles among these criteria are indistinguishable from that of Fig. 6(a). Figures 6(a) and 6(b) indicate that an energy point with a larger value of the DOS requires a larger number of iterations, because the KS dimension should be larger in order to distinguish individuals among densely distributed nearby states.

In Fig. 7(a), the decay behavior of the RN is plotted for the four chosen energy points that were already discussed in Figs. 1 and 6(a). When Fig. 7(a) and Fig. 1 are compared, one can see that the decay behavior of the RN is quite different among the four energy points but the ARN is universal, as it should be from Eq. (18). For example, we pick out the case in which the reference energy is chosen as the point labeled by B. In this case, the RN $\|r_n^{(j)}\|^2$ and the shift coefficient π_n^σ go to the extreme orders of 10^{-250} and 10^{+250} , respectively, at $n=300$. Even in such an extreme case, the computational procedure works well and the ARN follows the universal curve, as in Fig. 1.

Second, we discuss the convergence behavior of the Green's function including its *long-distance* component, unlike in Sec. III. For monitoring the convergence behavior, we should define the total residual norm (TRN), instead of the RN in Eq. (25), as

$$\|r_n^{(j)}\|^2 = \sum_i^M |i|r_n^{(j)}|^2, \quad (\text{A1})$$

where the elements are summed up among all the bases (M bases). In other words, the TRN shows the convergence be-

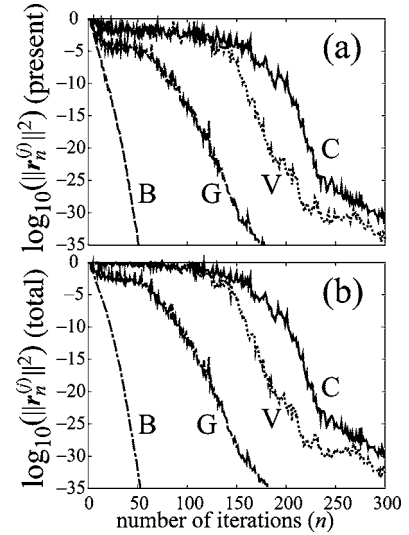


FIG. 7. Iteration dependence of (a) the residual norm (RN) in the present method and (b) the total residual norm (TRN). The symbols B, V, G, and C indicate the energy points that are shown by arrows in Fig. 6(a).

havior for all the elements of the Green's function $[G_{ij}$ or $G(\mathbf{r}, \mathbf{r}')$], including its long-distance components. We should recall that the RN in Eq. (25) is defined only for the short-distance components. The results are shown in Fig. 7(b), in which the decay behavior is slower than that in Fig. 7(a) at an earlier stage ($n \leq 30$), though the behavior is the same at later stages. The difference at the earlier stage appears because the accurate description of the Green's function at further distances needs a larger number of KS bases or a larger iteration number. Moreover, the computational cost is enormous to calculate all the elements of the Green's function, as shown in the SCOCG (total) case of Table I. The present discussion clarifies that only the short-distance components of the Green's function are required and calculated in practical applications.

2. Subspace diagonalization method

Here the subspace diagonalization method based on the KS (SDKS) method¹¹ is discussed for comparison with the shifted COCG method. Though the two methods, commonly, give the density matrix or Green's function within the KS, the difference between them comes from the computational cost and the effect of numerical round-off error.

The practical procedure of the SDKS method is summarized as follows. An orthogonal basis set for the KS is constructed by the Lanczos process, a three-term recurrence relation, $\{|K_1^{(j)}\rangle \equiv |j\rangle, |K_2^{(j)}\rangle, \dots, |K_v^{(j)}\rangle\}$.¹¹ Here the number of bases v is the dimension of the KS, $K_v(H, |j\rangle)$. This process creates simultaneously the reduced Hamiltonian matrix $H^{K(j)}$ within the KS $[(H^{K(j)})_{nm} \equiv \langle K_n^{(j)} | H | K_m^{(j)} \rangle]$, as a small tridiagonal matrix. Then the reduced matrix $H^{K(j)}$ is diagonalized and we obtain the eigenvalues $\varepsilon_\alpha^{(j)}$ and the coefficients $C_{\alpha n}^{(j)}$ ($\alpha = 1, 2, \dots, v$), where the eigenvectors are given as $|w_\alpha^{(j)}\rangle \equiv \sum_{n=1}^v C_{\alpha n}^{(j)} |K_n^{(j)}\rangle$. The Green's function is given as

$$\langle i|G|j\rangle \Rightarrow \sum_n^{\nu} \langle i|K_n^{(j)}\rangle \langle K_n^{(j)}|G_{\nu}^{(j)}|j\rangle \quad (\text{A2})$$

with the definition of

$$G_{\nu}^{(j)}(z) \equiv \sum_{\alpha}^{\nu} \frac{|w_{\alpha}^{(j)}\rangle \langle w_{\alpha}^{(j)}|}{z - \varepsilon_{\alpha}^{(j)}}. \quad (\text{A3})$$

The density matrix can be given in a similar manner.¹¹ The calculated band structure energy shows a rapid convergence as a function of the number of KS bases ν , in both semiconductor¹¹ and metal (fcc Cu, data not shown). In both cases, the result is well converged, typically, with $\nu=30$. We have simulated the reconstruction on a Si(001) surface,¹¹ as in Sec. IV A, and the resultant atomic positions or LDOSs agree with the ones obtained by the shifted COCG method.

Several differences in numerical treatment are found between the SDKS method and the shifted COCG method. The SDKS method gives the Green's function analytically in Eq. (A3) and its energy integration for the density matrix, Eq. (4), can be given also analytically, while the shifted COCG method gives the Green's function numerically on a given set of energy points and its energy integration should be carried out with a careful observation of the numerical error. Moreover, the computational cost of the SDKS method is smaller than, typically one-half of, that of the shifted COCG method, because the SDKS method requires only real vectors, such as $|K_n^{(j)}\rangle$, $|w_{\alpha}^{(j)}\rangle$, while the shifted COCG method requires several complex vectors, such as $|x_n^{(j)}\rangle$, $|r_n^{(j)}\rangle$.

Hereafter we discuss a crucial difference of the SDKS method from the shifted COCG method; the SDKS method shows a numerical instability with a very large number of KS bases (ν), owing to the accumulation of round-off error. The above instability is analyzed by introducing the RN with Eq. (23). An element of the RN is given as

$$\begin{aligned} \langle i|r_{\nu}^{(j)}\rangle &= \langle i|I - (z - H)G_{\nu}^{(j)}(z)|j\rangle \\ &= \langle i|j\rangle - \sum_{\alpha}^{\nu} \frac{\langle i|z - H|w_{\alpha}^{(j)}\rangle \langle w_{\alpha}^{(j)}|j\rangle}{z - \varepsilon_{\alpha}^{(j)}} \\ &= \langle i|j\rangle - \sum_{\alpha, n=1}^{\nu} \left(\frac{\langle i|z - H|K_n^{(j)}\rangle C_{\alpha n}^{(j)}}{z - \varepsilon_{\alpha}^{(j)}} \times \sum_{m=1}^{\nu} C_{\alpha m}^{(j)} \langle K_m^{(j)}|j\rangle \right). \end{aligned} \quad (\text{A4})$$

This quantity can be calculated with a negligible computational cost, since all the quantities in Eq. (A4), that is, $\{\varepsilon_{\alpha}^{(j)}\}$, $\{C_{\alpha n}^{(j)}\}$, $\{\langle i|K_n^{(j)}|\rangle\}$, and $\{\langle i|H|K_n^{(j)}|\rangle\}$, are always calculated in the generating procedure of the Green's function $G_{\nu}^{(j)}(z)$. The ARN $R_{\nu}^{(j)}$ can be defined in a similar way as in Eq. (27). The ARN was examined for a Si crystal in different system sizes (512, 4096, and 32 768 atoms), and the results are shown in Fig. 8. Here a problematic situation appears in the cases of 512 and 4096 atoms, because the ARN begins to grow after an appropriate value of the KS dimension ν . So as to analyze the growth of the error, the RN with the case of 512 atoms is shown in Fig. 9 with its energy dependence. The spectrum consists of only spikes before the growth of error [$\nu=30$, Fig.

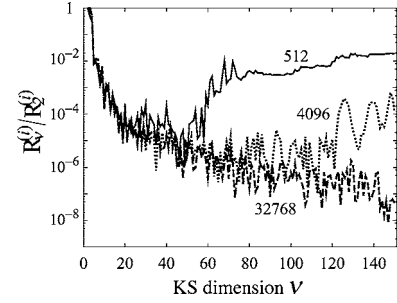


FIG. 8. Decay behavior of the ARN in the SDKS method for Si crystals with 512, 4096, and 32 768 atoms.

9(a)], while a finite background appears after the beginning of the growth of error [$\nu=100$, Fig. 9(b)].

The growth of error occurs because the loss of orthogonality ($\langle K_n^{(j)}|K_m^{(j)}\rangle \neq \delta_{nm}$) always happens in actual calculation after a long iteration of the Lanczos procedure, owing to the accumulation of round-off error. In such a case, the calculated eigenvectors $|w_{\alpha}^{(j)}\rangle$ have a finite deviation $|\xi_{\alpha}^{(j)}\rangle$ from the true eigenvectors:

$$H^{K(j)}|w_{\alpha}^{(j)}\rangle = \varepsilon_{\alpha}|w_{\alpha}^{(j)}\rangle + |\xi_{\alpha}^{(j)}\rangle. \quad (\text{A5})$$

Using Eqs. (A4) and (A5), we obtain

$$\begin{aligned} \langle i|r_{\nu}^{(j)}\rangle &= \langle i|I - (z - H)G_{\nu}^{(j)}(z)|j\rangle \\ &= \langle i|j\rangle - \sum_{\alpha}^{\nu} \frac{\langle i|z - H|w_{\alpha}^{(j)}\rangle \langle w_{\alpha}^{(j)}|j\rangle}{z - \varepsilon_{\alpha}^{(j)}} \\ &= \langle i|d\rangle + \sum_{\alpha=1}^{\nu} (\langle i|\xi_{\alpha}^{(j)}\rangle + \langle i|\delta H^{K(j)}|w_{\alpha}^{(j)}\rangle) \frac{\langle w_{\alpha}^{(j)}|j\rangle}{z - \varepsilon_{\alpha}^{(j)}}, \end{aligned} \quad (\text{A6})$$

where we define $\delta H^{K(j)} \equiv H - H^{K(j)}$ and use

$$|d\rangle \equiv |j\rangle - \sum_{\alpha=1}^{\nu} |w_{\alpha}^{(j)}\rangle \langle w_{\alpha}^{(j)}|j\rangle = \sum_{n=2}^{\nu} |K_n^{(j)}\rangle \langle K_n^{(j)}|K_1^{(j)}\rangle. \quad (\text{A7})$$

The last equality of Eq. (A7) is given by

$$\sum_{\alpha=1}^{\nu} |w_{\alpha}^{(j)}\rangle \langle w_{\alpha}^{(j)}| = \sum_{n=1}^{\nu} |K_n^{(j)}\rangle \langle K_n^{(j)}| \quad (\text{A8})$$

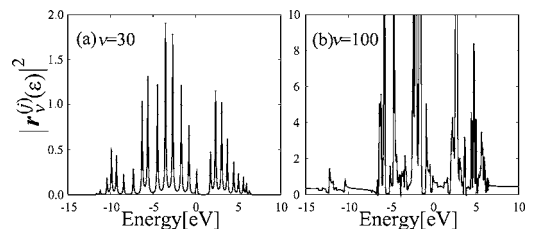


FIG. 9. Energy dependence of the RN in the subspace diagonalization method for a Si crystal with 512 atoms. The KS dimension is ν =(a) 30 and (b) 100.

and $|K_1^{(j)}\rangle \equiv |j\rangle$. The first and second terms in Eq. (A6) correspond to the finite background and the spikes in Fig. 9(b), respectively. With a small number of bases, as in Fig. 9(a), the orthogonality between the bases holds exactly and we

obtain $|d\rangle = |\xi_\alpha^{(j)}\rangle = 0$. Therefore, the energy-independent term, the first term of Eq. (A6), does not appear. The spikes in Fig. 9(a) appear because the reduced Hamiltonian matrix in the KS deviates from the original one ($\delta H^{K(j)} \equiv H - H^{K(j)} \neq 0$).

*Present address: Canon Inc., Analysis Technology Center, 30-2 Shimomaruko 3-chome, Ohta-ku, Tokyo 146-8501, Japan.

†Present address: Department of Computational Science and Engineering, Nagoya University, Furo-cho, Chikusa-ku, Nagoya 464-8603, Japan.

¹W. Kohn, Phys. Rev. Lett. **76**, 3168 (1996).

²R. Haydock, Solid State Phys. **35**, 129 (1980).

³G. Galli, Phys. Status Solidi B **217**, 231 (2000).

⁴S. Y. Wu and C. S. Jayamathi, Phys. Rep. **358**, 1 (2002).

⁵O. K. Andersen, T. Saha-Dasgupta, R. W. Tank, C. Arcangeli, O. Jepsen, and G. Krier, in *Electronic Structure and Physical Properties of Solids*, edited by H. Dressè (Springer-Verlag, Berlin, 2000), pp. 3–84.

⁶T. Hoshi and T. Fujiwara, J. Phys. Soc. Jpn. **69**, 3773 (2000).

⁷T. Hoshi and T. Fujiwara, Surf. Sci. **493**, 659 (2001).

⁸T. Hoshi and T. Fujiwara, J. Phys. Soc. Jpn. **72**, 2429 (2003).

⁹T. Hoshi, Ph.D. thesis, University of Tokyo, 2003.

¹⁰M. Geshi, T. Hoshi, and T. Fujiwara, J. Phys. Soc. Jpn. **72**, 2880 (2003).

¹¹R. Takayama, T. Hoshi, and T. Fujiwara, J. Phys. Soc. Jpn. **73**, 1519 (2004).

¹²T. Hoshi, Y. Iguchi, and T. Fujiwara, Phys. Rev. B **72**, 075323 (2005).

¹³S. Roche and D. Mayou, Phys. Rev. Lett. **79**, 2518 (1997).

¹⁴F. Triozon and S. Roche, Eur. Phys. J. B **46**, 427 (2005).

¹⁵T. Ozaki and K. Terakura, Phys. Rev. B **64**, 195126 (2001).

¹⁶H. A. van der Vorst, *Iterative Krylov Methods for Large Linear Systems* (Cambridge University Press, Cambridge, U.K., 2003).

¹⁷Y. Saad, *Iterative Methods for Sparse Linear Systems*, 2nd ed. (SIAM, Philadelphia, 2003).

¹⁸H. A. van der Vorst and J. B. M. Melissen, IEEE Trans. Magn. **26**, 706 (1990).

¹⁹A. Frommer, Computing **70**, 87 (2003).

²⁰The original paper (Ref. 19) gives the formulation for a general non-Hermitian matrix A , which is called the shifted Bi-CGStab algorithm. In the present context, however, the matrix A is complex symmetric and the present formulation of the shifted COCG algorithm can be adopted.

²¹I. Kwon, R. Biswas, C. Z. Wang, K. M. Ho, and C. M. Soukoulis, Phys. Rev. B **49**, 7242 (1994).

²²O. K. Andersen and O. Jepsen, Phys. Rev. Lett. **53**, 2571 (1984).

²³D. J. Chadi, Phys. Rev. Lett. **43**, 43 (1979).

²⁴A. Ramstad, G. Brocks, and P. J. Kelly, Phys. Rev. B **51**, 14504 (1995).

²⁵J. Pollman, P. Krüger, M. Rohlfing, M. Sabisch, and D. Vogel, Appl. Surf. Sci. **104-105**, 1 (1996).

²⁶R. Dronskowski and P. E. Blöchl, J. Phys. Chem. **97**, 8617 (1993).